

Computational search for Dirac and Weyl nodes in f -electron antiperovskites

Anna Pertsova,¹ R. Matthias Geilhufe,¹ Martin Bremholm,^{2,3} and Alexander V. Balatsky^{1,4}

¹*Nordita, KTH Royal Institute of Technology and Stockholm University,
Roslagstullsbacken 23, SE-106 91 Stockholm, Sweden*

²*Department of Chemistry and iNANO, Aarhus University, 8000 Aarhus, Denmark*

³*Center for Materials Crystallography, Aarhus University, 8000 Aarhus, Denmark*

⁴*Dept. of Physics, University of Connecticut, Storrs, CT 06269, USA*

(Dated: May 23, 2019)

We present the result of an *ab initio* search for new Dirac materials among inverse perovskites. Our investigation is focused on the less studied class of lanthanide antiperovskites containing heavy f -electron elements in the cation position. Some of the studied compounds have not yet been synthesized experimentally. Our computational approach is based on density functional theory calculations which account for spin-orbit interaction and strong correlations of the f -electron atoms. We find several promising candidates among lanthanide antiperovskites which host bulk Dirac states close to the Fermi level. Specifically, our calculations reveal massive three-dimensional Dirac states in materials of the class A_3BO , where $A=Sm, Eu, Gd, Yb$ and $B=Sn, Pb$. In materials with finite magnetic moment, such as Eu_3BO ($B=Sn, Pb$), the degeneracy of the Dirac nodes is lifted, leading to appearance of Weyl nodes.

I. INTRODUCTION

Dirac materials (DMs) is a growing class of materials which exhibit a linear, Dirac-like spectrum of quasi-particle excitations [1]. Examples of DMs that have attracted particular attention in the past decade include graphene [2], three-dimensional (3D) topological insulators (TIs) [3, 4], topological crystalline insulators (TCIs) [5], and the newly discovered three-dimensional DMs such as Dirac [6, 7] and Weyl semimetals [8–10]. Over the past several years, it has been suggested that a new subclass of DMs can be found in cubic antiperovskite materials [11–15]

Antiperovskites, or inverse perovskites, are inorganic compounds with a perovskite type structure in which the positions of cations and anions are interchanged. The typical structure is A_3BX , where A is an electropositive cation, B is a divalent metallic anion and X is a monovalent anion i.e. the position of A and X are reversed compared to ordinary perovskites. Antiperovskites have a great potential for electronic, magnetic and thermoelectric applications [16].

Regarding the search for DMs, much focus has been on antiperovskite oxides with a simple cubic structure, A_3BO , where A is an alkaline earth metal such as Ca, Ba, Sr . The prototypical example is Ca_3PbO which was proposed as a potential DM in a number of studies [12–15]. Recently, superconductivity has been reported in a similar compound, the antiperovskite Dirac-metal oxide Sr_3SnO with hole doping [17]. There has been an increasing interest in other antiperovskite materials. A group of nitride antiperovskites with a common structure A_3BiN , where $A=Ca, Ba, Sr$ has been predicted to be 3D TIs when subject to properly designed uniaxial strain [12]. A recent density functional theory (DFT) based study of a larger class of alkaline earth pnictides A_3BX , where $A=Ca, Ba, Sr$ and $B, X=N, P, As, Sb, Bi$ found several materials that can be driven into topological phases by

properly engineered strain [18]. A promising candidate is Ca_3BiP which is a topological semimetal without strain but can be driven into a 3D TI or a Dirac semimetal phase.

The nature of the Dirac states in antiperovskite materials predicted so far has been studied from different viewpoints. Initially, the data mining search based on electronic structure calculations performed in Ref. [11] identified Ca_3PbO (and similar compounds, A_3BO , $A=Ca, Ba, Sr$ and $B=Sn, Pb$) as a possible 3D TI. More specifically, it was suggested to be a strong 3D TI based on apparent band inversion at the Γ point. The band inversion was confirmed in other studies [12, 14, 19]. However, despite the band inversion, the product of parities of the bands at time-reversal invariant momenta remains the same with or without spin orbit coupling (SOC). Therefore, based on the parity criterion [20], strain free Ca_3PbO is a trivial insulator. Properly engineered uniaxial strain can change the ordering of the inverted bands, turning the material into a 3D TI, similarly to Ca_3BiN [12]. In the absence of strain, the Ca_3PbO family was predicted to be TCI with unusual surface states with open Fermi surface similar to Weyl semimetals [14, 15]. At the same time, it was suggested that Ca_3PbO is a massive 3D DM, with Dirac nodes occurring in the 3D Brillouin away from any high-symmetry point [13, 19, 21–23].

In fact, the topological gap at Γ and the 3D Dirac states away from Γ may coexist in these materials. Based on topological band theory, Hsieh *et al.* [14] showed that the band inversion at the Γ point, responsible for the TCI phase in Ca_3PbO , leads to the appearance of a gapped node (avoided crossing) along the Γ - X direction of the 3D Brillouin zone. This feature was studied in detail by Kariyado and Ogata [13, 19] using a combination of *ab initio* and tight-binding methods. In particular, it was shown that these states can be described as massive Dirac fermions. Photoemission experiments are required to verify these theoretical predictions.

More recent theoretical work has predicted the existence of Dirac nodal lines in materials with weak SOC, which can be realized in some antiperovskite compounds [24, 25]. Specifically, Yu *et al.* [24] found that in the absence of SOC, Cu_2PdN is a nodal-line semimetal with three nodal circles due to cubic symmetry. Nodal lines originate from the band inversion at the R point of the 3D Brillouin zone and are protected by time reversal and inversion symmetries [26]. Inclusion of SOC drives the system into a Dirac semimetal phase with three pairs of Dirac nodes. Similar conclusions were found by Kim *et al.* [25] for a more general case of Cu_2N doped with non-magnetic transition metal atoms, i.e. in $\text{Cu}_3\text{X}_x\text{N}$ (antiperovskite structure) with $\text{X}=\text{Ni}, \text{Cu}, \text{Zn}, \text{Pd}, \text{Ag}, \text{Cd}$. In particular, two maximally-doped cases, Cu_3PdN and Cu_3ZnN were studied with effective Hamiltonian and *ab initio* methods, demonstrating bulk Dirac nodal lines and nearly-flat surface states.

We note that the existence of nodal lines is not a universal property of antiperovskites. Since it requires vanishing or weak spin-orbit interaction, it is not realized in compounds containing elements with very large atomic numbers. On the other hand, band inversion at time reversal invariant momenta and the occurrence of nodes along adjacent symmetry lines is a common feature. Unlike in 3D TIs, the band inversion in antiperovskites is not due to SOC but can be induced by changing the lattice constant or the chemical elements. The details of the electronic structure, such as the character of the inverted bands and the position of the Dirac nodes are material specific.

In this work we focus on the scarcely studied group of lanthanide antiperovskite oxides, A_3BO , where $\text{A}=\text{Sm}, \text{Eu}, \text{Gd}, \text{Yb}$ and $\text{B}=\text{Sn}, \text{Pb}$. Among published work, Yb_3SnO and Yb_3PbO were predicted to be 3D TIs [11]. In a recent work based on a large-scale *ab initio* search for topological materials, Yb_3PbO has been identified as a possible TCI. [27] Based on electronic structure calculations, we find that this group of compounds is characterized by massive Dirac nodes in the 3D Brillouin zone. The most interesting candidates are Eu_3SnO , Eu_3PbO , Yb_3SnO and Yb_3PbO which have Dirac states near the Fermi level. Among these materials, Yb_3PbO is the most promising for further studies and applications since the Dirac states are isolated from other bands. The origin of the 3D Dirac states is similar to the case of Ca_3PbO . Our DFT calculations show that most of the considered lanthanide antiperovskites possess a finite magnetic moment due to unpaired f -electrons in their outer shells (Yb_3BO is an exception due to the filled f -shell of Yb). This offers intriguing possibilities of combining magnetism and Dirac fermion physics in pristine materials without doping or proximity effects. Furthermore, in magnetic lanthanide antiperovskites, e.g. Eu_3BO ($\text{B}=\text{Sn}, \text{Pb}$), based on the number of the nodes and the band degeneracy, we identify the nodes in the 3D Brillouin zone as massive Weyl nodes.

The paper is organized as follows. In Sec. II we provide

computational details. Section III reports the outcome of our *ab initio* search for DMs among lanthanide antiperovskites. Namely, we summarize the results of electronic structure calculations for the materials of this class in the bulk phase. Several candidates displaying Dirac/Weyl states are identified. The electronic structure of the most promising candidates with isolated cones near the Fermi level are discussed in more detail. We also analyze the character and the possible origin of the Dirac states using a specific example of Yb_3PbO . Finally, we draw some conclusions in Sec. IV.

II. METHODS

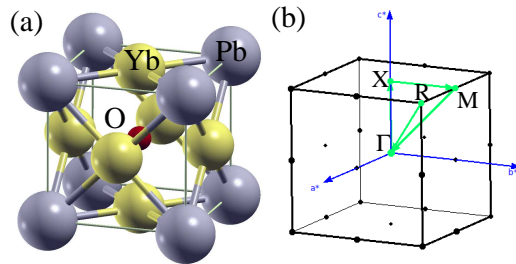


FIG. 1. (a) The cubic antiperovskite structure of Yb_3PbO . (b) Γ -X-M- Γ path in the Brillouin zone used for bandstructure calculations.

We performed DFT calculations using the full-potential all-electron linearized augmented plane-waves method as implemented in the Wien2k *ab initio* package [28]. The Perdew-Burke-Ernzerhof generalized gradient approximation (PBE-GGA) [29] is used for the exchange correlation functional. For lanthanide antiperovskites, the GGA+U method was used to account for local correlations at the cation site. The Hubbard U parameter in the GGA+U approach effectively describes the on-site repulsion associated with the narrow $3d$ or $4f$ bands. We used the following arguments to choose a suitable value of U for our calculations of lanthanide antiperovskites.

In a standard GGA calculation with $U=0$, the $4f$ band appears right at the Fermi level. A finite U pushes the band away from the Fermi level into the valence band. Since the experimental data for $4f$ valence states is not available, it is sufficient to choose the value of U such as (i) the $4f$ band is pushed down into the valence band, (ii) varying U in a reasonable range does not affect the electronic states at the Fermi level, in particular the Dirac nodes. We performed test calculations for one of the compounds (Yb_3PbO) with U ranging from 3eV to 12eV. We verified that changing U does not affect the nodes, while it shifts the narrow $4f$ states to lower energy. The overall bandstructure around the Fermi level also does not change appreciably. Furthermore, comparing total energies of the system calculated with different U, we found that $U=10$ eV corresponds to a local minimum of the

total energy. We also noted that for $U=8$ and 9 eV, the arrangement of bands in the vicinity of the Γ point is slightly different compared to other cases. For all other values of U , the bands in the energy window $[-2$ eV, 2 eV] are essentially identical. Hence, we choose $U=10$ eV, which is within the commonly accepted range for rare earths [30] and, in particular, lanthanides. [31–33].

We used 126 non-equivalent k -points in a $10 \times 10 \times 10$ mesh of the first Brillouin zone for self-consistent calculations. SOC is included in all calculations as it can not be ignored in heavy-element compounds. Geometry optimization was performed to find the equilibrium lattice constant, which is particularly important for compounds for which no experimental structural data is available (Sm_3SnO , Sm_3PbO , Gd_3SnO , Gd_3PbO). The Brillouin zone path used for bandstructure calculations is shown in Fig. 1(b).

The results of structural (volume) optimization together with experimental (estimated or observed) lattice constants for lanthanide antiperovskites are presented in Table I. For compounds that have been synthesized and for which structural data can be found in the literature (Eu_3SnO , Eu_3PbO , Yb_3SnO , Yb_3PbO), the DFT optimized lattice constants are close to experimental values. We use experimental lattice parameters [34, 35] for the existing lanthanide antiperovskites, as well for the test data set of alkali antiperovskites [35, 36].

TABLE I. Experimental and DFT optimized lattice constant for lanthanide antiperovskite oxides: A_3BO , $\text{A}=\text{Sm}$, Eu , Gd , Yb , and $\text{B}=\text{Sn}$, Pb ; space group $\text{P}\bar{m}3\text{m}$. E(O) refers to estimated (observed) structural data. References are given for the experimental lattice constants.

System	Experiment, a (\AA)	DFT, a (\AA)
Sm_3SnO	5.111 (E)	4.984
Sm_3PbO	5.124 (E)	5.015
Eu_3SmO	5.077 (O) [35]	5.018
Eu_3PbO	5.091 (O) [35]	5.051
Gd_3SnO	5.043 (E)	4.851
Ga_3PbO	5.058 (E)	4.887
Yb_3SnO	4.837 (O) [34]	4.804
Yb_3PbO	4.859 (O) [34]	4.842

III. RESULTS AND DISCUSSION

We use the well studied Ca_3PbO group of antiperovskite oxides containing alkali metals as a test set for our *ab initio* search. The results are summarized in Table II [see also the electronic structure for Ca_3PbO in Fig. 4(a,b)]. The table includes information on the presence (+) or absence (-) of Dirac nodes according to our DFT electronic structure calculations, as well as the availability of structural data (synthesis), and references

to previous theoretical work with a brief note on the predicted character of the Dirac states.

Our results for the Ca_3PbO family are in agreement with Kariyado and Ogata [13]. Namely, we find gapped nodes formed by linearly dispersing bands along the Γ - X direction in all compounds of this group. The nodes are located at the Fermi level. In Ba_3SnO and Ba_3PbO , there are other states crossing the Fermi level thus obscuring the Dirac states. The results also largely agree with Hsieh *et al.* [14], with the possible exception of Ca_3SnO .

TABLE II. Possible Dirac materials (DMs) in antiperovskite oxides with alkali metals: A_3BO , $\text{A}=\text{Ca}$, Ba , Sr , $\text{B}=\text{Sn}$, Pb ; space group $\text{P}\bar{m}3\text{m}$.

System	DM	Synthesis	Theory
Ba_3PbO	+	[34–36]	[11](3DTI), [12](3DTI+strain), [13](3DDM), [14](TCI)
Ba_3SnO	-	[34–36]	[11–14]
Ca_3PbO	+	[34–36]	[11](3DTI), [12](3DTI+strain), [13](3DDM), [14](TCI)
Ca_3SnO	+	[34–36]	[11](3DTI), [13](3DDM), [14](TCI)
Sr_3PbO	+	[34–36]	[11](3DTI), [12](3DTI+strain), [13](3DDM), [14](TCI)
Sr_3SnO	+	[34–36]	[11](3DTI), [14](TCI)

We now focus on lanthanide antiperovskite oxides. The results of the electronic structure calculations for this group of materials are summarized in Table III, where we also include the information on the value of the calculated magnetic moment (for lanthanide atoms in the unit cell). The available experimental and theoretical literature is considerably more scarce compared to the Ca_3PbO family. Structural data is available for Eu_3BO and Yb_3BO ($\text{B}=\text{Sn}$, Pb), while for Sm_3BO and Gd_3BO ($\text{B}=\text{Sn}$, Pb), we use the lattice constant obtained from DFT (see Table I).

TABLE III. Possible Dirac materials (DMs) in lanthanide antiperovskite oxides: A_3BO , $\text{A}=\text{Sm}$, Eu , Gd , Yb , $\text{B}=\text{Sn}$, Pb ; space group $\text{P}\bar{m}3\text{m}$.

System	DM	Magnetic moment (μ_B)	Synthesis	Theory
Sm_3PbO	-	5.8	-	-
Sm_3SnO	-	5.7	-	-
Eu_3PbO	+	6.9	[34]	-
Eu_3SnO	+	6.9	[34]	-
Gd_3PbO	-	7.1	-	-
Ga_3SnO	-	7.2	-	-
Yb_3PbO	+	0	[35]	[11](3DTI)
Yb_3SnO	+	0	[35]	[11](3DTI)

Based on bulk electronic structure, we conclude that Eu_3BO and Yb_3BO ($\text{B}=\text{Sn}$, Pb) are 3D DMs with a finite

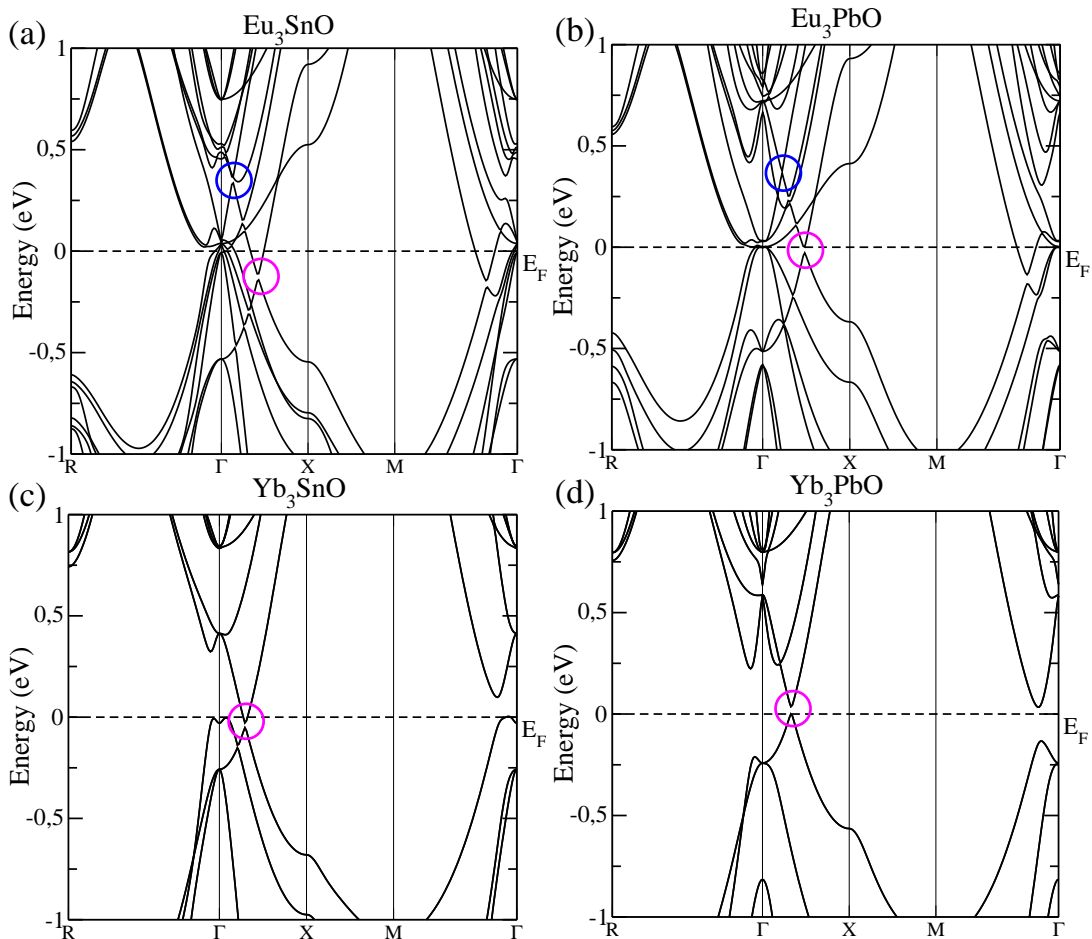


FIG. 2. Calculated bandstructures of cubic lanthanide antiperovskites (a) Eu_3SnO , (b) Eu_3PbO , (c) Yb_3SnO , and (d) Yb_3PbO . SOC is included in the calculations. The horizontal dashed line marks the position of the Fermi level. Circles highlight possible massive Dirac/Weyl fermion features along the Γ -X direction.

Dirac gap. The calculated bandstructures of these materials are presented in Fig. 2. Here we refer to 3D DM as materials having nodes (in general, gapped) in their 3D Brillouin zone, regardless of the nature of the nodes and their degeneracy. However, there is an important distinction between non magnetic (Yb_3BO) and magnetic (Eu_3BO) systems. Since magnetic ground state breaks time-reversal symmetry, we expect the degeneracy of the Dirac nodes to be lifted in magnetic lanthanide antiperovskites, giving rise to gapped Weyl nodes. Below we will discuss in more detail the bandstructures for these two cases.

Yb_3SnO and Yb_3PbO do not show any sizable magnetic moment, which is expected since Yb has a fully filled f -shell. These materials are characterized by a single node located along the Γ -X symmetry direction (X is the center of the face in the perovskite structure). Due to cubic symmetry, there are in total six nodes along the six equivalent Γ -X paths parallel to $\pm\mathbf{a}$, $\pm\mathbf{b}$ and $\pm\mathbf{c}$, where \mathbf{a} , \mathbf{b} , \mathbf{c} are reciprocal lattice vectors. The degeneracy of the bands forming the nodes is $g = 2$. Hence we identify the nodes in Yb_3BO as Dirac nodes. The energy gap at

the node is $\Delta \approx 24$ meV for Yb_3SnO and $\Delta \approx 40$ meV for Yb_3PbO . The case of Yb_3PbO is particularly interesting as it has an isolated Dirac node at the Fermi level. In Yb_3SnO , the node is located slightly below the Fermi level.

In our spin-polarized DFT calculations for magnetic lanthanide perovskites, we considered a ferromagnetic ground state, e.g. we assumed that magnetic moments of the lanthanide atoms, e.g. Eu in Eu_3BO ($\text{B}=\text{Sn}$, Pb), are parallel to each other. The calculated magnetic moments are equal for all magnetic atoms in the unit cell and are close to the magnetic moments of the cations, e.g. $\approx 7 \mu_B$ for Eu^{2+} . This is the simplest and the most feasible choice for our computational approach and it is partly justified by experimental measurements [37]. Such calculations could also represent a paramagnetic phase in external magnetic field, where all spins align parallel to each other.

It should be mentioned that magnetic coupling in realistic materials is likely to be more complicated. In the cubic antiperovskite structure, the lanthanide cations are located at the face-centered positions, forming the central

octahedron [see Fig. 1(a)]. Hence, the lattice is formed by triangular net of the magnetic moments. Such structure is prone to magnetic frustration and can lead to a complicated magnetic state with many possible phases. This has been documented in other materials with similar structure, for example in Mn-based antiperovskite nitrides, Mn_3XN ($\text{X} = \text{Ga}, \text{Zn}, \text{Cu}, \text{Ge}, \text{Sn}$), which display multiple magnetic interactions below the temperature of the paramagnetic transition. [38]

An experimental study of magnetism and transport in Eu-based antiperovskites has been reported in Ref. [37]. Interestingly, the magnetization measurements in Eu_3BO ($\text{B} = \text{Sn}, \text{Pb}$) did not confirm the anticipated magnetic frustration (the frustration factor extracted from the temperature dependence of the magnetization was found to be close to unity, meaning no frustration). At the same time, the materials become antiferromagnetic at low temperatures, with the Neel temperature of 33 K in Eu_3SnO and 43 K for Eu_3PbO . To reconcile antiferromagnetism with the apparent absence of frustration, a model of magnetic periodic sublattices was suggested. In this model, the crystal consists of parallel sublattices (planes), inside which the magnetic moments of lanthanide ions interact ferromagnetically, while between the planes the moments interact antiferromagnetically. Magnetic sublattices appear as steps in the field-dependent magnetization curves which has been confirmed in the experiment. The resulting phase diagram for Eu_3BO ($\text{B} = \text{Sn}, \text{Pb}$) reveals several magnetic ordered states with temperature- and field-dependent phase transitions between the states.

Based on the assumption of a ferromagnetic ground state, we find that Eu_3SnO and Eu_3PbO have a total magnetic moment of $\approx 21 \mu_B$ and a magnetic moment on Eu site of $\approx 6.9 \mu_B$. The direction of the magnetic moment is along [001]. Based on a simple model of a 4×4 Dirac Hamiltonian in external magnetic field, the Dirac node is split into two Weyl nodes, separated in momentum space by a vector proportional to the magnetic field vector [39] Assuming that the magnetization acts as an effective magnetic field, we expect the shifted Weyl nodes to appear along the Γ - X direction parallel to $+\mathbf{c}$, which we refer to as Γ - X_c . The path used for bandstructure calculations presented in Fig. 2 includes Γ - X_c [see Fig. 1(b)].

One can see in Fig. 2(a,b) that Eu_3BO indeed displays nodes along the $\Gamma - X_c$ directions. There is a gapped node, which is similar in shape and location to Yb_3BO , located at the Fermi level in Eu_3PbO and at ≈ 100 meV below the Fermi level in Eu_3SnO [marked with magenta circle in Fig. 2(a,b)]. The energy gap at the node is $\Delta \approx 25$ meV. Apart from this node, there are many other avoided band crossings near the Fermi level. One possible node at ≈ 300 meV above the Fermi level is marked with blue circles in Fig. 2(a,b). We find a smaller energy gap at this node, $\Delta \approx 1$ meV for Eu_3SnO and $\Delta \approx 10$ meV for Eu_3PbO . To further clarify the position of the nodes, we plot in Fig. 3 the bandstructures of Eu_3BO along two non-equivalent paths, Γ - X_c and Γ - X_a (parallel to $+\mathbf{a}$).

The node at positive energy (blue circles) is clearly absent in the bandstructure plotted along Γ - X_a . We verified that the band degeneracy around the gapped nodes is $g = 1$. The number of nodes and the degeneracy indicate that the nodes in Eu_3BO could be identified as Weyl nodes.

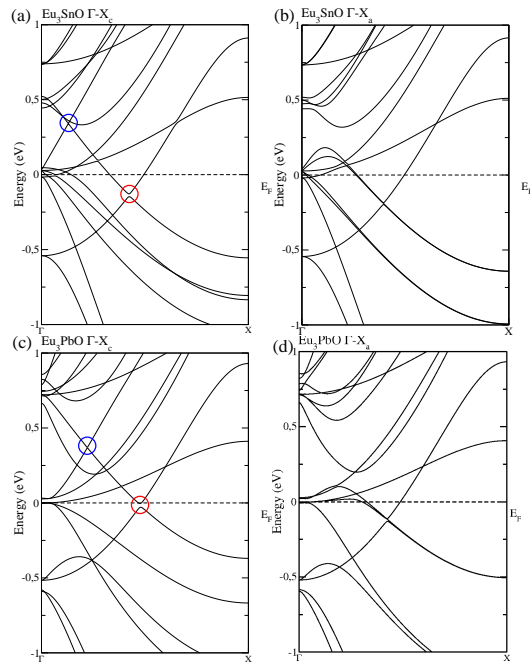


FIG. 3. Calculated bandstructures of magnetic lanthanide antiperovskites (a,b) Eu_3SnO and (c,d) Eu_3PbO along two non-equivalent paths Γ - X_c (left) and Γ - X_a (right). Possible Weyl nodes shifted along the Γ - X_c direction are marked by circles in panels (a) and (c).

In order to precisely identify the Weyl nodes, further bulk and surface calculations are required. This is outside the scope of the present work since our goal is to identify potential 3D DM candidates. It is worth pointing out that the expectations based on the 4×4 Dirac Hamiltonian do not necessarily hold in realistic materials. Villanova and Park [40] showed, using an *ab-initio*-based tight-binding model, that in Ni_3Bi Dirac semimetal the Dirac node is split into four Weyl nodes when magnetic field is applied. Moreover, a finite magnetization in intrinsically magnetic materials is not equivalent to external magnetic field.

Next, we comment on the possible origin of bulk Dirac states in lanthanide antiperovskite oxides. For this we compare the character of the low energy states for the typical alkali antiperovskite oxide Ca_3PbO and Yb_3PbO (see Fig. 4). It was noted in Refs. [13, 19] that the low energy Dirac states in Ca_3PbO are formed mainly by Ca $3d$ and Pb $6p$ orbitals. Among Ca $3d$, the $3d_{x^2-y^2}$ orbitals give the major contribution to the Dirac states. We have verified this picture [see the electronic structure of Ca_3PbO with band character in Fig. 4(a,b)].

Based on the insight from DFT electronic structure,

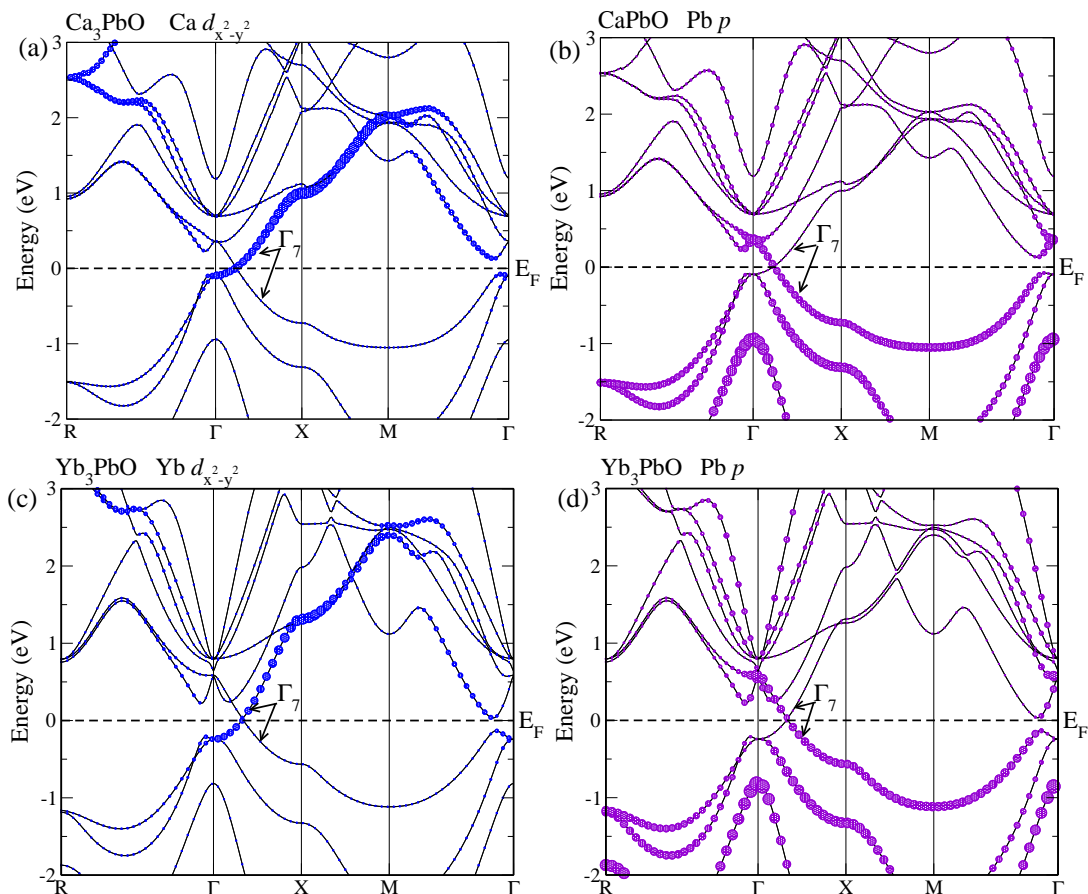


FIG. 4. Band character of cubic alkali antiperovskite (a,b) Ca_3PbO and lanthanide antiperovskite (c,d) Yb_3PbO . Filled circles show relative contributions of Ca and Yb d -states (a,c) and Pb p states (b,d). Only $d_{x^2-y^2}$ states are shown for Ca and Yb. We have verified that the contribution of other d orbitals with different symmetry is negligible at low energies. In panels (c) and (d), the highly localized Yb $4f$ states are located below -2eV . The horizontal dashed line marks the position of the Fermi level. Irreducible representations are shown for valence and conduction bands along the Γ -X direction.

Kariyado and Ogata [13, 19] constructed a tight-binding Hamiltonian with a basis formed by Ca $d_{x^2-y^2}$ and Pb p states, which the authors proved to be a Dirac Hamiltonian yielding 3D gapless Dirac states along the Γ -X line. It was suggested that a small gap at the Dirac node (few tens of meV's) is due to SOC and the coupling to other states away from the Fermi level i.e. Pb $5d$ and other Ca $3d$ states [19]. We have verified in our calculations that in the absence of SOC, the Dirac states are gapless. Further analysis of the DFT bands for Ca_3PbO with SOC reveals that the two bands forming the node along the Γ -X direction belong to the same irreducible representation, Γ_7 of the C_{4v} double point group [see Fig. 4(a,b)], which further justifies the avoided crossing between these bands (irreducible representation have been computed with Wien2k [28] and independently verified with QUANTUM ESPRESSO [41, 42]).

SOC is also responsible for the band inversion at the center of the Brillouin zone which was found in Ca_3PbO [13, 14, 19]. Since Ca d and Pb p states, which give rise to low-energy electronic states, have different parities, there exist two possible band orderings at the Γ

point. In the normal ordering, the d orbitals of Ca (A position in A_3BO) lie above the Pb p orbitals (B position in A_3BO). However, in the presence of SOC the order is reversed, namely the top of the p bands lies above the bottom of the d bands. This band inversion signals a possible topological phase which was detected by Klintenberg *et al.* [11]. However, it leaves the materials a trivial insulator in the Z_2 classification of TIs because the product of parity eigenvalues remains unchanged due to the four-fold degeneracy of valence and conduction band extrema at Γ [12, 19].

Nevertheless, the inverted band ordering is an important ingredient in the low-energy effective Hamiltonian of Ref. [19] which produces 3D Dirac states away from Γ . It was subsequently demonstrated by Hsieh *et al.* [14] that this band inversion leads to a TCI phase described by a nonzero mirror Chern number. It was also shown that the bulk Dirac node is a direct consequence of the band inversion at Γ i.e. the band crossing on the Γ -X is absent in the trivial phase characterized by normal band ordering [14]. This is different from the band inversion at the R point in Cu_3PdN , which involves p and d states

of the metallic anion (Pd 5*p* states are lower than Pd 4*d* states). When SOC is included, Cu₃PdN exhibits Dirac nodes along *R-X* and *R-M* directions, where the node along *R-M* remains gapless [24]. Similarly, the band inversion at *X* in Cu₃ZnN leads to nodes along *R-X* and *R-M* [25].

We find that the character of low energy states in Yb₃PbO is similar to Ca₃PbO [see Fig. 4(c,d)]. In this case, the Dirac states are formed mainly by Yb 4*d*_{*x*²-*y*²} and Pb 6*p* orbitals. The valence and conduction bands along Γ -*X* belong to the same irreducible representation, Γ_7 of the C_{4v} group. These are strong indications that the origin of the Dirac states in this material is similar to Ca₃PbO. Hence, we conclude that Yb₃PbO is characterized by massive 3D Dirac fermions at finite *k* and is also a potential TCI. Further theoretical and experimental work will be useful to describe bulk Dirac states and possible topological surface states due to the TCI phase in this material and other lanthanide antiperovskites with similar properties.

Since the above discussion concerned non-magnetic antiperovskites, we also checked the character of the bands for magnetic Eu₃BO (see Fig. 5). The features in the bandstructures that we identified as potential Weyl nodes do not have exactly the same band character as the Dirac node in Yb₃PbO. However, they do have contributions from Eu *d* and Sn/Pb *p* states.

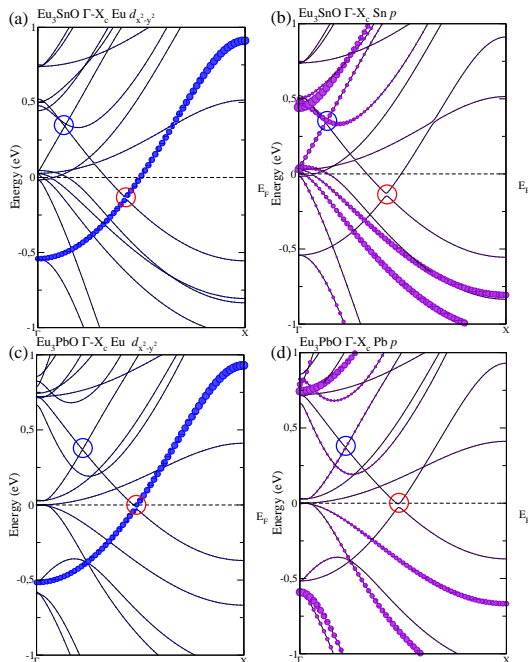


FIG. 5. Band character of magnetic antiperovskite (a,b) Eu₃SnO and (c,d) Eu₃PbO. Filled circles show relative contributions Eu *d*-states (a,c) and Sn/Pb *p* states (b,d). Bands are plotted along the Γ -*X*_{*c*} path.

Finally, we also considered hypothetical structures

A₃BO, A=Gd, Sm and B=Sn, Pb, for which no experimental structural data is available to date. For these compounds, we have obtained DFT optimized crystal structures (see Table I), however their dynamic structural stability needs to be investigated further. Although our calculations showed interesting features, including band crossings near the Fermi level, we were not able to clearly identify 3D Dirac states in these compounds.

IV. CONCLUSION

In conclusion, we performed an *ab initio* search for Dirac materials among some antiperovskite oxides. Our data set includes both the Ca₃PbO family as a test subset and the less studied lanthanide antiperovskites containing *f*-electron elements, some of which have not been synthesized to date. For the Ca₃PbO family (A₃BO, A=Ca, Ba, Sr, B=Sn, Pb), our electronic structure calculations show gapped 3D Dirac states, which is consistent with previous theoretical work. Among the *f*-electron antiperovskites, we identify Eu₃BO and Yb₃BO (B=Sn, Pb) as 3D DMs, which display massive Dirac nodes along the Γ -*X* in the 3D Brillouin zone.

In Yb₃BO (B=Sn, Pb) the nodes are energetically close to the Fermi level and the energy gap at the nodes is few tens of meV's. Yb₃PbO is particularly promising as it has an isolated Dirac node at the Fermi level. Eu₃BO (B=Sn, Pb) possess a finite magnetic moment due to unfilled *f*-electron shell. We find that in these magnetic lanthanide antiperovskites the degeneracy of the Dirac nodes can be lifted, leading to appearance of Weyl nodes in the 3D Brillouin zone. As demonstrated previously for Ca₃PbO family, the existence of bulk Dirac states at finite *k* is a direct consequence of the band inversion at the center of the 3D Brillouin zone, which gives rise to a TCI phase. Hence, the 3D DMs found among the *f*-electron antiperovskites may be potential TCIs.

V. ACKNOWLEDGMENTS

We are grateful to P. Hofmann for useful discussion. This work was supported by the VILLUM FONDEN via the Centre of Excellence for Dirac Materials (Grant No. 11744), the European Research Council under the European Unions Seventh Framework Program (FP/2207-2013)/ERC Grant Agreement No. DM-321031, the Swedish Research Council Grant No. 638-2013-9243, and the Knut and Alice Wallenberg Foundation. The authors acknowledge computational resources from the Swedish National Infrastructure for Computing (SNIC) at the High Performance Computing Center North (HPC2N)

- [1] T. Wehling, A. M. Black-Schaffer, and A. V. Balatsky, *Advances in Physics* **63**, 1 (2014).
- [2] A. H. Castro Neto, F. Guinea, N. M. R. Peres, K. S. Novoselov, and A. K. Geim, *Rev. Mod. Phys.* **81**, 109 (2009).
- [3] M. Z. Hasan and C. L. Kane, *Rev. Mod. Phys.* **82**, 3045 (2010).
- [4] X.-L. Qi and S.-C. Zhang, *Rev. Mod. Phys.* **83**, 1057 (2011).
- [5] L. Fu, *Phys. Rev. Lett.* **106**, 106802 (2011).
- [6] S. M. Young, S. Zaheer, J. C. Y. Teo, C. L. Kane, E. J. Mele, and A. M. Rappe, *Phys. Rev. Lett.* **108**, 140405 (2012).
- [7] M. Neupane, S.-Y. Xu, R. Sankar, N. Alidoust, G. Bian, C. Liu, I. Belopolski, T.-R. Chang, H.-T. Jeng, H. Lin, A. Bansil, F. Chou, and M. Z. Hasan, *Nature Communications* **5**, 3786 (2014).
- [8] X. Wan, A. M. Turner, A. Vishwanath, and S. Y. Savrasov, *Phys. Rev. B* **83**, 205101 (2011).
- [9] S.-M. Huang, S.-Y. Xu, I. Belopolski, C.-C. Lee, G. Chang, B. Wang, N. Alidoust, G. Bian, M. Neupane, C. Zhang, S. Jia, A. Bansil, H. Lin, and M. Z. Hasan, *Nature Communications* **6**, 7373 (2015).
- [10] S.-Y. Xu, I. Belopolski, N. Alidoust, M. Neupane, G. Bian, C. Zhang, R. Sankar, G. C. Chang, Z. Yuan, C.-C. Lee, S.-M. Huang, H. Zheng, J. Ma, D. S. Sanchez, B. Wang, A. Bansil, F. Chou, P. P. Shibayev, H. Lin, S. J. Jia, and M. Z. Hasan, *Science* **349**, 613 (2015).
- [11] M. Klintonberg, J. Haraldsen, and A. Balatsky, *Applied Physics Research* **6**, 31 (2014).
- [12] Y. Sun, X.-Q. Chen, S. Yunoki, D. Li, and Y. Li, *Phys. Rev. Lett.* **105**, 216406 (2010).
- [13] T. Kariyado and M. Ogata, *Journal of the Physical Society of Japan* **80**, 083704 (2011), <http://dx.doi.org/10.1143/JPSJ.80.083704>.
- [14] T. H. Hsieh, J. Liu, and L. Fu, *Phys. Rev. B* **90**, 081112(R) (2014).
- [15] C.-K. Chiu, Y.-H. Chan, X. Li, Y. Nohara, and A. P. Schnyder, *Phys. Rev. B* **95**, 035151 (2017).
- [16] M. Bilal, S. Jalali-Asadabadi, R. Ahmad, and I. Ahmad, *Journal of Chemistry* **2015**, 495131 (2015).
- [17] M. Oudah, A. Ikeda, J. N. Hausmann, S. Yonezawa, T. Fukumoto, S. Kobayashi, M. Sato, and Y. Maeno, *Nat. Comm.* **7**, 13617 (2016).
- [18] W. F. Goh and W. E. Pickett, *Phys. Rev. B* **97**, 035202 (2018).
- [19] T. Kariyado and M. Ogata, *Journal of the Physical Society of Japan* **81**, 064701 (2012), <http://dx.doi.org/10.1143/JPSJ.81.064701>.
- [20] L. Fu and C. L. Kane, *Phys. Rev. B* **76**, 045302 (2007).
- [21] T. Kariyado, *Three-Dimensional Dirac Electron Systems in the Family of Inverse-Perovskite Material Ca₃PbO* (The University of Tokyo, Tokyo, 2012).
- [22] T. Kariyado, *Journal of Physics: Conference Series* **603**, 012008 (2015).
- [23] Y. Fuseya, M. Ogata, and H. Fukuyama, *Journal of the Physical Society of Japan* **81**, 013704 (2012), <http://dx.doi.org/10.1143/JPSJ.81.013704>.
- [24] R. Yu, H. Weng, Z. Fang, X. Dai, and X. Hu, *Phys. Rev. Lett.* **115**, 036807 (2015).
- [25] Y. Kim, B. J. Wieder, C. L. Kane, and A. M. Rappe, *Phys. Rev. Lett.* **115**, 036806 (2015).
- [26] H. Weng, Y. Liang, Q. Xu, R. Yu, Z. Fang, X. Dai, and Y. Kawazoe, *Phys. Rev. B* **92**, 045108 (2015).
- [27] T. Zhang, Y. Jiang, Z. Song, H. Huang, Y. He, Z. Fang, H. Weng, and C. Fang, *Nature* **566**, 475 (2019).
- [28] P. Blaha, K. Schwarz, G. K. H. Madsen, D. Kvasnicka, and J. Luitz, *WIEN2K, An Augmented Plane Wave Plus Local Orbitals Program for Calculating Crystal properties* (Vienna University of Technology, Austria, 2001).
- [29] J. P. Perdew, K. Burke, and M. Ernzerhof, *Phys. Rev. Lett.* **77**, 3865 (1996).
- [30] D. van der Marel and G. A. Sawatzky, *Phys. Rev. B* **37**, 10674 (1988).
- [31] M. Pang, Y. Zhan, H. Wang, W. Jiang, and Y. Du, *Comput. Mater. Sci.* **50**, 3303 (2011).
- [32] Z. Khadraoui, K. Horchani-Naifer, and M. Ferhi, *Opt. Mater.* **47**, 484 (2015).
- [33] Z. Khadraoui, K. Horchani-Naifer, M. Ferhi, and M. Ferid, *Chem. Phys.* **457**, 37 (2015).
- [34] A. Velden and M. Jansen, *Zeitschrift für anorganische und allgemeine Chemie* **630**, 234, <https://onlinelibrary.wiley.com/doi/pdf/10.1002/zaac.200300313>.
- [35] J. Nuss, C. Mühle, K. Hayama, V. Abdolazimi, and H. Takagi, *Acta Cryst.* **B71**, 300 (2015).
- [36] A. Widera and H. Schäfer, *Materials Research Bulletin* **15**, 1805 (1980).
- [37] V. Abdolazimi, "Inverse-perovskites eu3to (t=si, ge, sn, pbo): Magnets" (2014).
- [38] Y. S. Sun, Y. F. Guo, X. X. Wang, W. Yi, J. J. Li, S. B. Zhang, C. I. Sathish, A. A. Belik, and K. Yamaura, *Journal of Physics: Conference Series* **400**, 032094 (2012).
- [39] Consider the Dirac Hamiltonian $H_D = \tau_z \otimes v_F \mathbf{k} \cdot \sigma$, where v_F is the Fermi velocity, σ and τ are Pauli matrices. Interaction with an effective magnetic field \mathbf{b} can be written as $H_b = -\tau_0 \otimes \sigma \cdot \mathbf{b}$. Then the eigenstates of the Hamiltonian $H = H_D + H_b$ are given by $E_{\pm}^{\xi} = \pm v_F |(\mathbf{k} - \xi \mathbf{k}_0)|$, where $\xi = \pm 1$ and $\mathbf{k}_0 = \mathbf{b}/v_F$. This gives two Weyl nodes with chiralities ξ , separated by vector $2\mathbf{k}_0$.
- [40] J. W. Villanova and K. Park, *Phys. Rev. B* **98**, 075123 (2018).
- [41] P. Giannozzi, S. Baroni, N. Bonini, M. Calandra, R. Car, C. Cavazzoni, D. Ceresoli, G. L. Chiarotti, M. Cococcioni, I. Dabo, A. D. Corso, S. de Gironcoli, S. Fabris, G. Fratesi, R. Gebauer, U. Gerstmann, C. Gougoussis, A. Kokalj, M. Lazzeri, L. Martin-Samos, N. Marzari, F. Mauri, R. Mazzarello, S. Paolini, A. Pasquarello, L. Paulatto, C. Sbraccia, S. Scandolo, G. Sclauzero, A. P. Seitsonen, A. Smogunov, P. Umari, and R. M. Wentzcovitch, *Journal of Physics: Condensed Matter* **21**, 395502 (2009).
- [42] P. Giannozzi, O. Andreussi, T. Brumme, O. Bunau, M. B. Nardelli, M. Calandra, R. Car, C. Cavazzoni, D. Ceresoli, M. Cococcioni, N. Colonna, I. Carnimeo, A. D. Corso, S. de Gironcoli, P. Delugas, R. A. D. Ferretti, A. Floris, G. Fratesi, G. Fugallo, R. Gebauer, U. Gerstmann, F. Giustino, T. Gorni, J. Jia, M. Kawamura, H.-Y. Ko, A. Kokalj, E. Kkbenli, M. Lazzeri, M. Marsili, N. Marzari, F. Mauri, N. L. Nguyen, H.-V. Nguyen, A. O. de-la Roza, L. Paulatto, S. Ponc, D. Rocca, R. Sabatini, B. Santra, M. Schlipf, A. P. Seitsonen, A. Smogunov, I. Timrov, T. Thonhauser, P. Umari, N. Vast, X. Wu, and S. Baroni,

